GEOPHYSICAL RESEARCH LETTERS, VOL. 24, NO. 16, PAGES 1979-1982, AUGUST 15, 1997

Ionospheric response to an auroral substorm

R. W. Schunk, L. Zhu, J. J. Sojka, and M. D. Bowline

Center for Atmospheric and Space Sciences, Utah State University, Logan, Utah

Abstract. The response of the ionosphere to a representative auroral substorm was simulated. The response was found to be significant at all altitudes in a large spatial region near midnight magnetic local time. In this midnight region, there were T_e and T_i hot spots, substantial $O^+ \rightarrow NO^+$ composition changes, non-Maxwellian velocity distributions, transient ion upwellings, a large-scale lowering of the F-layer, ionization peaks that occur in the E-region, and sharp horizontal gradients. Also, during the expansion phase, the E-region densities increase due to auroral precipitation, while the plasma densities above 300 km decrease due to the overall lowering of the ionosphere. The net result is that the temporal morphologies of the plasma densities at high and low altitudes are opposite during this part of the substorm. These complex features indicate that care must be exercised when interpreting plasma measurements from both ground-based and space-based instruments.

1. Introduction

Substorms correspond to the explosive release of energy in the auroral region near midnight magnetic local time [*Akasofu*, 1964; *McPherron et al.*, 1973]. Following onset, there are growth, expansion and recovery phases, with the expansion phase typically lasting about 30 minutes and the entire substorm about 2-3 hours. When viewed via the associated optical emission, the substorm first appears as a localized region of bright emission on the poleward edge of the auroral oval near local magnetic midnight. The so-called bulge is part of the westward traveling surge that occurs during the expansion phase of a substorm. Associated with the substorms are locally enhanced electric fields, particle precipitation, and both field-aligned and electrojet currents. Also, intense discrete auroral arcs typically appear near the poleward and westward fronts of the bulge. Eventually, the substorm associated disturbances encompass the entire high-latitude region [cf. *Fujii et al.*, 1994; *Sánchez et al.*, 1996].

Numerous models have been invoked to explain the occurrence of substorms. The most common model includes a growth phase during which magnetic flux is transported from the dayside magnetosphere to the tail [*Hones*, 1979]. Subsequently, the increased magnetic stress in the tail leads to a thinning of the plasma sheet and then to reconnection. When the oppositely directed magnetic fields above and below the equatorial plane reconnect in an x-line configuration, there is a sudden conversion of magnetic energy into particle acceleration in the central plasma sheet (the expansion phase). The flows are toward the Earth on the earthward side of the x-line. However, *Rostoker and Eastman* [1987] argue that substorm signatures can be explained via the coupling of the ionosphere to the plasma sheet and low-latitude boundary layers. In the model of *Lui* [1979], a current disruption is invoked to explain the onset of substorms. In this model, the plasma sheet thins because a sudden reduction in the cross-tail current launches a tailward propagating fast MHD rarefaction wave. On the other hand, *Roux* [1985] attributes substorm onset to a Rayleigh-Taylor instability at the boundary between dipole-like and tail-like magnetic field lines in the inner plasma sheet region. Currents flowing along the instability surface couple the ionosphere and magnetosphere. *Kan et al.* [1988] proposed a model in which the nonlinear coupling of the magnetosphere-ionosphere (M-I) system plays an important role in substorm onset. Specifically, following a southward turning of the interplanetary magnetic field (IMF) there is enhanced magnetospheric convection, but the M-I system adjusts to the new convection state via Alfven wave reflections between the ionosphere and magnetosphere. The ionospheric Hall and Pedersen conductances, which evolve in time, affect the Alfven wave reflection characteristics, and hence, the ionosphere plays an active role in the onset and development of a substorm.

Our interest is not in rigorously modeling a substorm, but in calculating the detailed ionospheric response to a substorm. To do this, we need self-consistent plasma convection and particle precipitation patterns throughout the polar region during the substorm. The patterns must have a fairly good spatial resolution (at least 100 km) and a very good temporal resolution (~ sec.). Although some impressive multi-instrument measurements (radars, satellites, magnetometers) of substorm evolution have recently been made [*Kamide et al.*, 1994; *Sánchez et al.*, 1996], they are still not adequate with regard to providing the sharp convection reversals, the narrow precipitation features, the self-consistency, and the rapid temporal evolution that are needed for ionospheric modeling. Therefore, we used a substorm model similar to that proposed by *Kan et al.* [1988] and *Kan and Sun* [1996] to generate the magnetospheric drivers that are needed for our ionospheric simulation of a "representative" substorm.

2. Ionospheric and Substorm Models

The USU time-dependent ionospheric model (TDIM) is a multi-species NO^+, O_2^+, N_2^+, O^+, N^+, He^+ model that is based on a numerical solution of the coupled continuity, momentum, and energy equations [*Schunk*, 1988; *Sojka*, 1989]. The TDIM is a Lagrange-Euler hybrid model in that the equations are solved as a function of altitude for horizontally convecting plasma flux tubes. The 3-dimensional nature of the model is obtained by following numerous flux tubes in a given simulation. However, the TDIM requires several global inputs, with the primary ones being the atmospheric parameters and the magnetospheric convection and precipitation patterns. For

Paper number 97GL01252.
0094-8534/97/97GL-01252$05.00

the substorm simulation, the MSIS atmospheric model was adopted and the conditions chosen were near winter solstice (day 330), low solar activity ($F_{10.7}$ = 100) and Ap = 15 for the prestorm magnetic activity level. The thermospheric wind was obtained from the *Hedin* [1991] empirical model using the same input parameters that were used for the MSIS model.

The time-dependent convection and precipitation patterns were obtained from the substorm model described by *Zhu and Kan* [1990], with the physical scenario closely following that proposed by *Kan et al.* [1988] and *Kan and Sun* [1996]. In this substorm model, the growth phase is initiated by an increase in the magnetospheric convection that is driven by enhanced reconnection at the dayside magnetopause due to a southward turning of the IMF. Alfven waves are launched in association with the enhanced convection and they provide the coupling between the ionosphere and magnetosphere during the substorm. In the transient period, when the Alfven waves bounce back and forth between the ionosphere and magnetosphere, the plasma convection, particle precipitation, and field-aligned currents increase with time. Eventually, at the end of the transient period, the enhanced M-I coupling leads to the onset of a substorm. Further details concerning this substorm model will be given in a future publication.

3. Substorm Simulation and Ionospheric Response

For the substorm simulation presented here, the spatial resolution was 100 km and the time step was 5 seconds. The convection and precipitation patterns were calculated for magnetic latitudes greater than 50° in the northern hemisphere. Initially, a set of quiet-time convection and precipitation patterns was calculated by running the substorm model for a sufficiently long time to reach the asymptotic state. The growth phase of the substorm commenced at 1200 UT when the Alfven wave associated with the enhanced convection that was initiated at the dayside magnetopause reached the ionosphere. The growth phase lasted for 24 minutes, and the expansion phase reached its peak 11 minutes later (1235 UT). Only the first 35 minutes of the substorm were simulated because our goal was to elucidate the ionospheric response at the time the substorm disturbance was the greatest.

Figure 1 shows snapshots of two of the important drivers of ionospheric dynamics, the precipitating electron energy flux and the magnitude of the convection electric field. The snapshots are for 1200 UT (pre-substorm) and 1235 UT (expansion phase). For the 1235 UT plots, the pre-storm values have been subtracted from the results so that the enhancements associated with the substorm can be clearly seen. Before the substorm, the maximum values for the energy flux and electric field in the substorm region (74° latitude, 21.5 MLT) are 0.3 erg/cm^2/s and 5 mV/m, respectively, while during the expansion phase the maximum values approach 7 erg/cm^2/s and 50 mV/m (Note the maximum electric field occurs at a slightly different location). The plots of the precipitation's characteristic energy (not shown) are qualitatively very similar to the energy flux plots, and the maximum characteristic energies in the substorm region are 0.5 keV (pre-substorm) and 7 keV (expansion phase). The Hall conductance in the nocturnal auroral region increases by a factor of 15 during the substorm, reaching 25 mho. An important feature to note is that during the substorm the regions where the precipitation and electric field maximize are not colocated.

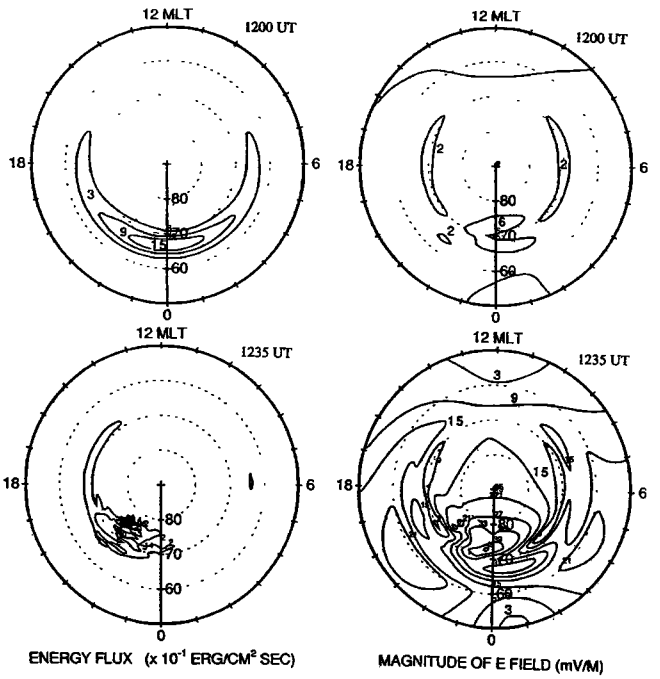

Figure 1. Auroral electron energy flux and E-field magnitude at 1200 UT (top) and 1235 UT (bottom). For the 1235 UT plots, the pre-substorm values (at 1200 UT) have been subtracted so that only the substorm enhancements are shown. At 1200 UT, the maximum energy flux and E-field are 1.5 erg/cm^2/s and 10 mV/m, respectively, while at 1235 UT the maximum energy flux and E-field are 7 erg/cm^2/s and 50 mV/m. In the 1235 UT plots, the gradients are too steep for the individual contours to be seen, but our purpose is simply to show where the steep gradients are.

For the ionospheric model, the quiet-time (asymptotic state) convection and precipitation patterns were used initially and the model was run until a self-consistent (diurnally reproducible) ionosphere was obtained. Then, at 1200 UT, the substorm simulation commenced and the ionospheric model received an updated set of convection-precipitation patterns every 30 seconds. The outputs of the model were the electron and ion densities, drift velocities, and temperatures (T_e, $T_{i\parallel}$, $T_{i\perp}$) over the altitude range from 90 to 800 km and for all latitudes greater than 50° magnetic. The simulation indicated that the substorm had a significant effect on the ionosphere at all altitudes and that the effect was the largest during the expansion phase. In response to the substorm, there were separate T_e and T_i hot spots, substantial $O^+ \rightarrow NO^+$ composition changes, non-Maxwellian velocity distributions, a large-scale lowering of the F-layer, electron density enhancements in the E-region and depletions in the F-region and topside, ion upwelling, and steep horizontal gradients.

Plate 1 shows snapshots of T_i (200 km) and T_e (600 km) at both 1200 UT (pre-storm) and 1235 UT (expansion phase). The peak ion heating occurs near 200 km and is due to ion-neutral frictional interactions as the ions convect through the slower moving neutral gas. Before the substorm, the T_i distribution is fairly uniform, with T_i in the 700-800 K range. During the expansion phase, T_i is elevated in the midnight sector between 2100-0200 MLT and 65-80° latitude. The region of high T_i coincides with the region of large electric fields (Figure 1), and in the area where the electric field

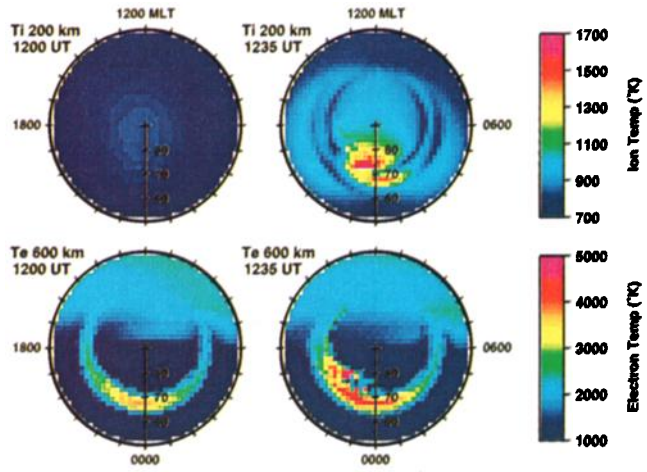

Plate 1. Snapshots of the T_i (200 km) and T_e (600 km) distributions at 1200 UT (pre-substorm) and 1235 UT (expansion phase).

approaches 50 mV/m, T_i increases to almost 2000 K. On the other hand, T_e is elevated in the regions where electron precipitation occurs, and these regions are typically adjacent to the regions where the E-field is large. Consequently, as shown in Plate 1, the T_e and T_i "hot spots" are close to each other, but are separate regions.

Associated with the elevated T_i is a substantial $O^+ \rightarrow NO^+$ composition change owing to the energy dependence of the $O^+ + N_2 \rightarrow NO^+ + N$ reaction rate [*Schunk et al.*, 1975]. However, an $O^+ \rightarrow NO^+$ conversion also occurs due to a lowering of the ionosphere in the regions where there is a downward $\mathbf{E} \times \mathbf{B}$ drift component. The net effect of both processes is shown in Plate 2, where snapshots of $n(O^+)$ and $n(NO^+)$ at 300 km are shown at both 1200 UT (pre-substorm) and 1235 UT (expansion phase). Note that where the E-field is large, $n(O^+)$ is decreased and $n(NO^+)$ is increased. Note also that $n(NO^+)$ is increased over a large region that extends beyond the regions where the E-field is large. At 300 km, which as we will show later is above the layer peak, the NO^+ density amounts to 30-40% of the total ion density in a large spatial region near midnight during the expansion phase of the substorm.

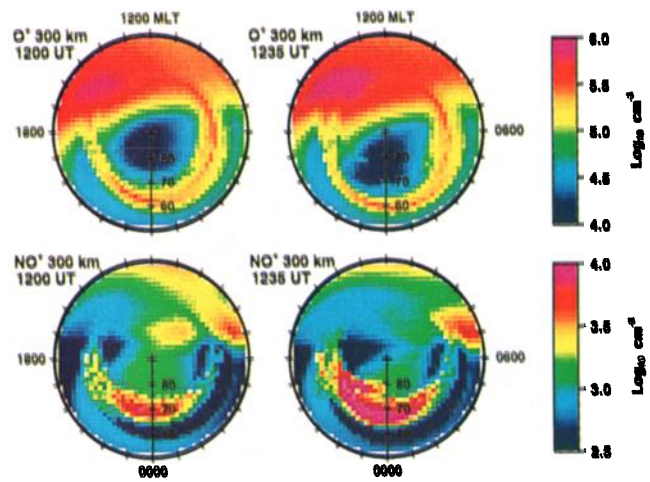

Plate 2. Snapshots of the O^+ and NO^+ densities at 300 km and at 1200 UT (pre-substorm) and 1235 UT (expansion phase).

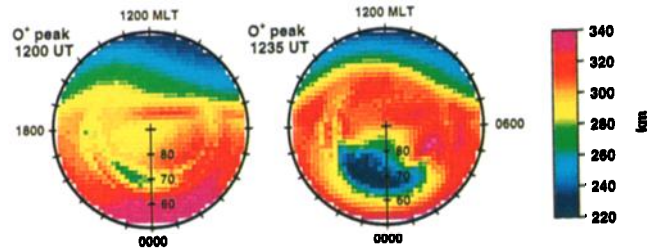

Plate 3. Snapshots of the height of the maximum O^+ density at 1200 UT (pre-substorm) and 1235 UT (expansion phase).

The $O^+ \rightarrow NO^+$ conversion that occurs in regions of both elevated T_i and downward $\mathbf{E} \times \mathbf{B}$ drifts leads to a substantial lowering of the O^+ peak height during the substorm, as shown in Plate 3. The O^+ peak is decreased from about 280 km to about 220 km in a large region near midnight during the substorm. Also, in this midnight region, NO^+ is the dominant ion at the ionization maximum. This is shown in Figure 2, where altitude profiles of the plasma densities and temperatures are shown at 1235 UT in both T_e and T_i "hot spot" regions. In these regions, which are separated by about 300 km, the layer peak is in the E-region and NO^+ is the dominant ion at the peak. Also note that T_i is anisotropic (non-Maxwellian) in the hot spots, with $T_{i\perp} > T_{i\parallel}$; $T_i = (T_{i\parallel} + 2T_{i\perp})/3$ [cf. *St.-Maurice and Schunk*, 1979]. The anisotropy is largest at low altitudes where the ion-neutral frictional heating is the largest. The decrease in the anisotropy with altitude is primarily due to the isotropic scattering associated with Coulomb collisions, which increase in importance with altitude. Finally, when the hot spots first develop, there is a large-scale ion upwelling (not shown) as the topside plasma scale heights adjust to the enhanced ion and electron temperatures.

During the substorm expansion phase, the electron density (N_e) increases at E-region altitudes in an extended region near midnight due to auroral precipitation. However, in the same region, N_e decreases at altitudes between about 300-800 km (not shown), with the result that the N_e temporal morphology during the substorm is "opposite " at high and low altitudes. The density decrease at altitudes above about 300 km results from the lowering of the ionosphere and consequent increased recombination (Plate 3 and Figure 2).

4. Summary

The response of the ionosphere to a representative substorm was simulated. An electrodynamical model of the coupled magnetosphere-ionosphere system was first used to calculate convection, precipitation, and current patterns during the substorm. These patterns, which were global, time-dependent and self-consistent, provided the inputs for a detailed calculation of the ionospheric response to a substorm. The ionospheric model provided 3-dimensional distributions of the ion and electron densities, drift velocities, and temperatures at altitudes between 90-800 km and for latitudes greater than 50° magnetic, with a 4 km vertical resolution, a 100 km horizontal resolution, and a 30 second temporal resolution.

The simulation indicated that there is a significant ionospheric response to a substorm at all altitudes. During the expansion phase, there is a large spatial region near midnight MLT that is disturbed. In this location the following occurs:

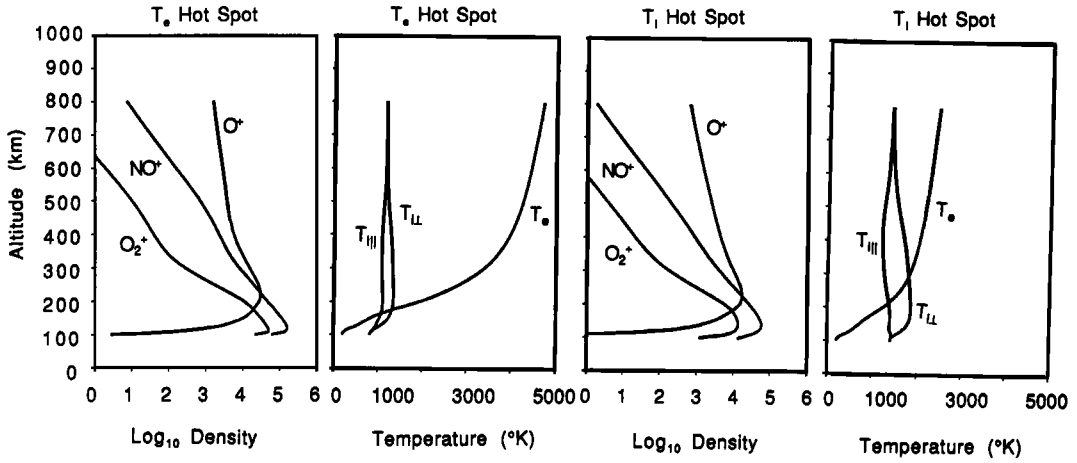

Figure 2. Altitude profiles of the plasma densities and temperatures at both T_e (68.1° latitude, 22.9 MLT) and T_i (71.6° latitude, 22.6 MLT) hot spot locations during the expansion phase of the substorm.

(1) There is a large-scale lowering of the ionosphere, which acts to reduce electron densities above about 300 km and increase them at low altitudes; (2) Localized T_e and T_i hot spots form, in which there are anisotropic ion temperature distributions ($T_{i\perp} > T_{i\parallel}$); (3) Major $O^+ \rightarrow NO^+$ composition changes occur; (4) The maximum ionization peak can be in the E-region; (5) Transient ion upwellings develop in response to both particle and Joule heating; and (6) Sharp horizontal gradients exist.

The sharp horizontal gradients, non-Maxwellian velocity distributions, and ion composition changes that occur during a substorm can have a significant effect on the interpretation of ground-based measurements from both optical instruments and radars. Also, the opposite temporal morphologies of the plasma densities at high and low altitudes could affect the interpretation of in situ satellite measurements. Hopefully, the features presented here will be useful not only for providing model predictions that can be tested, but for providing cautions on data interpretations.

Acknowledgement. This research was supported by NASA grant NAG5-1484, ONR grant N00014-95-1-0652 and NSF grant ATM-9612638 to Utah State University.

References

Akasofu, S.-I., The development of the auroral substorm, *Planet. Space Sci., 12*, 273-282, 1964.

Fujii, R., R. A. Hoffman, P. C. Anderson, J. Craven, M. Sugiura, L. A. Frank and N. C. Maynard, Electrodynamic parameters in the nighttime sector during auroral substorms, *J. Geophys. Res., 99*, 6093-6112, 1994.

Hedin, A. E., et al., Revised model of thermospheric winds using satellite and ground-based observations, *J. Geophys. Res., 96*, 7657-7688, 1991.

Hones, E. W., Jr., Transient phenomena in the magnetotail and their relationship to substorms, *Space Sci. Rev., 23*, 393, 1979.

Kamide, Y., A. D. Richmond, B. A. Emery, C. F. Hutchins, B.-H. Ahn, O. de la Beaujardiere, J. C. Foster, R. A. Heelis, H. W. Kroehl, R. J. Rich, and J. A. Slavin, Ground-based studies of ionospheric convection associated with substorm expansion, *J. Geophys. Res., 99*, 19451-19466, 1994.

Kan, J. R. and W. Sun, Substorm expansion phase caused by an intense localized convection imposed on the ionosphere, *J. Geophys. Res., 101*, 27271-27281, 1996.

Kan, J. R., L. Zhu and S.-I. Akasofu, A theory of substorms: Onset and subsidence, *J. Geophys. Res., 93*, 5624, 1988.

Lui, A. T. Y., Observations of plasma sheet dynamics during magnetospheric substorms, in *Dynamics of the Magnetosphere*, edited by S.-I. Akasofu, P. 563, D. Reidel, Norwell, MA, 1979.

McPherron, R. L., C. T. Russell and M. P. Aubry, Satellite studies of magnetospheric substorms on August 15, 1968. 9. Phenomenological model for substorms, *J. Geophys. Res., 78*, 3131-3149, 1973.

Rostoker, G., and T. Eastman, A boundary layer model for the magnetospheric substorms, *J. Geophys. Res., 92*, 12187, 1987.

Roux, A., Generation of field-aligned current structures at substorm onsets, *Proceedings of ESA Workshop on Future Missions in Solar, Heliospheric and Space Plasma Physics, Eur. Space Agency, Spec. Publ. ESA SP-235*, 151, 1985.

Sánchez, E. R., J. M. Ruohoniemi, C.-I. Meng and E. Friis-Christensen, Toward an observational synthesis of substorm models: Precipitation regions and high-latitude convection reversal observed in the nightside auroral oval by DMSP satellite and HF radars, *J. Geophys. Res., 101*, 19801-19837, 1996.

Schunk, R. W., A mathematical model of the middle and high latitude ionosphere, *PAGEOPH, 127*, 255-303, 1988.

Schunk, R. W., W. J. Raitt, and P. M. Banks, Effect of electric fields on the daytime high-latitude E and F regions, *J. Geophys. Res., 80*, 3121, 1975.

Sojka, J. J., Global scale, physical models of the F region ionosphere, *Rev. Geophys., 27*, 371-403, 1989.

St.-Maurice, J.-P., and R. W. Schunk, Ion velocity distributions in the high latitude ionosphere, *Rev. Geophys., 17*, 99-134, 1979.

Zhu, L. and J. R. Kan, Effects of ionospheric recombination time scale on the auroral signature of substorms, *J. Geophys. Res., 95*, 10389-10398, 1990.

M. D. Bowline, R. W. Schunk, J. J. Sojka, and L. Zhu, Center for Atmospheric and Space Sciences, Utah State University, Logan, UT 84322-4405. (e-mail: schunk@cc.usu.edu; sojka@fasojka.cass.usu.edu; zhu@cc.usu.edu)

(Received February 21, 1997; accepted April 14, 1997 .)